Journal of Manufacturing Processes 124 (2024) 377–384

Contents lists available at ScienceDirect

Journal of Manufacturing Processes

journal homepage: www.elsevier.com/locate/manpro

On the mechanisms of charge weld evolution in aluminum extrusion

Eren Can Sariyarlioglu, Torgeir Welo, Jun Ma *

Department of Mechanical and Industrial Engineering, Norwegian University of Science and Technology, Trondheim 7491, Norway

ARTICLE INFO

Keywords:
Aluminum extrusion
Charge weld
Transverse weld
Front-end defect
Material integrity

ABSTRACT

This study aims to provide new insights into the governing mechanisms of material property evolution within the charge weld zone in the hot extrusion process of aluminum profiles. A set of 6xxx series aluminum alloy tubular profiles was produced through carefully designed industrial experiments of billet-to-billet extrusion. The evolution of material integrity within the charge weld zones was experimentally characterized by microhardness tests, optical microscopy, scanning electron microscopy (SEM), and drift-expansion tests. The experimental analyses reveal that the material integrity of charge welds gradually increases from the onset to the end, primarily driven by the 'local' pressure history experienced. Towards the end of the charge weld zone, grooves and holes, and oxide particles gradually vanish, leading to enhanced material integrity. A through-process finite element (FE) model was developed using QForm-Extrusion software to analyze the thermo-mechanical history of charge weld formation, providing a deeper understanding of how material properties evolve and the underlying mechanisms governing this evolution. The model was experimentally validated in terms of the extrusion load and distribution of the charge welds in extruded profiles. Overall, the new insights gained in this study offer valuable knowledge for enhancing the process and quality control in billet-to-billet extrusion, as well as reducing in-process scrap towards more sustainable production of aluminum profiles.

1. Introduction

Billet-to-billet extrusion provides high overall process efficiency, enabling cost-effective production of long-length, hollow aluminum profiles. However, this industrial method involves continuous material flow between consecutive aluminum billets, which leads to the formation of a transition zone, known as charge weld in the extruded profile (Fig. 1). Charge weld is a solid-state pressure weld between the mating surfaces of two successive billets [1]. In an ideal scenario, where the merging surfaces of both billets have no aluminum oxide layer and exhibit identical mechanical properties, the configuration could be classified as non-defective [2]. In a real-world industrial scenario, however, oxidation inevitably does exist on the billet surfaces, accompanied by the presence of lubricant and oxidized metal residues on the butt-end surface initiated from the shear blade. The combination of oxidation and undesirable residues can introduce discontinuities in the extruded profile, ultimately leading to a charge weld zone with substandard mechanical properties and material integrity [2,3]. In industrial practice, thus, up to 20% of the extruded length influenced by the charge weld is removed from the rest of the profile and then recycled as in-process scrap [4]. Therefore, it is crucial to understand the governing mechanisms that affect the material integrity within the charge weld zone, for achieving increased material yield, carbon neutrality as well as reduced cost.

In this context, Valberg [1] contributed a comprehensive review of aluminum extrusion welds up to 1998, offering insights into understanding the mechanisms underlying charge welds. The material integrity of charge welds was investigated by Loukus et al. [6], revealing a disparity in terms of ductility between the extruded parent material and charge weld zone. However, the underlying reasons for these variations in mechanical test results remain unexplored. In a separate investigation, Zhang et al. [7] examined the difference in microstructural characteristics of the charge weld zone. The findings indicate that the new material within charge welds comprises equiaxed coarse grains, while the old material is characterized by elongated recrystallized grains. Subsequent studies conducted by Ren et al. [8] and Zhang et al. [9] affirmed the consistency of the microstructural observations with Zhang et al. [7], asserting that the new material in the charge weld zone exhibits recrystallized courser grains. Den Bakker et al. [3] dived into the failure mode and mechanical properties in the transition zone. The authors stated that the mechanical properties of the transition zone are determined by the density of the oxide particles at the interface between

* Corresponding author.
E-mail address: jun.ma@ntnu.no (J. Ma).

https://doi.org/10.1016/j.jmapro.2024.06.022
Received 14 May 2024; Accepted 10 June 2024

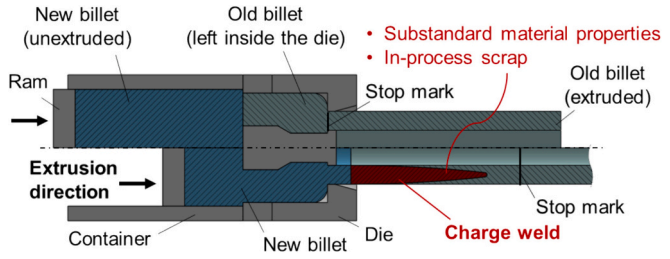

Fig. 1. Schematic view of charge weld formation in a porthole die extrusion process (adapted from Sariyarlioglu et al. [5]).

the old material and new material, albeit without providing detailed insights into the presence of oxide particles. In another study on the microstructure and material integrity of charge welds, Yu et al. [10] pointed out that the non-circular charge weld shapes result in enhanced weld quality; however, the charge-weld quality is inferior to that of longitudinal seam welds. Recently, Oberhausen and Cooper [11] developed an analytical model to predict the charge-weld strength, successfully capturing certain observed experimental trends. However, the predictive accuracy of the model necessitates further refinement due to the potential influence of impurities, oxide particles and lubricant within the charge weld.

The current state of research on charge-weld material integrity in aluminum extrusion reveals a significant knowledge gap, particularly in understanding how the deformation history and mechanisms related to the charge weld zone affect the mechanical integrity and properties of the product. This in combination with different extrusion die geometries obviously makes the control of material integrity within the charge weld zone, and consequently the optimization of extrusion process, very challenging in industrial practice. Therefore, it is imperative to effectively control the charge weld and thus improve both the efficiency and sustainability aspects of aluminum extrusion.

The remainder of this paper is structured as follows: Section 2 describes the industrial extrusion process, along with the experiments conducted for the characterization of the material integrity within the charge weld zone. In addition, the numerical model development for reproducing the formation of charge weld and thermal-mechanical histories is presented. Section 3 outlines the discussion of the findings from both conducted experimental and numerical analyses to comprehend the governing mechanisms of material integrity within charge weld. Finally, a conclusion of the key findings and suggestions for future research are summarized in Section 4.

2. Experiments and modeling

2.1. Industrial-scale extrusion experiments

Billet-to-billet extrusion experiments were conducted at Benteler Automotive in Raufoss, utilizing a 22 MN industrial extrusion press to manufacture tubular aluminum profiles. The production material, billet, was AA6060, and its detailed chemical composition can be found in Table 1.

The billet was produced through the DC-casting method and subsequently homogenized prior to extrusion operation. In each batch, a total of 60 billets were consecutively extruded, with the specific process parameters outlined in Table 2. Following the extrusion operation, the resulting profiles were promptly quenched and then stored at room temperature for several days.

Table 1
Chemical composition of AA6060 in weight% [12].

Si	Fe	Cu	Mn	Mg
0.30–0.6	0.10–0.3	≤0.10	≤0.10	0.35–0.6
Zn	Ti	Al	Cr	Others
≤0.15	≤0.10	Bal.	≤0.05	≤0.15

2.2. Characterization of charge welds

Charge welds of aluminum profiles produced from industrial experiments under steady-state operational conditions were investigated, with a specific focus on the transition zone between the 10th and 11th positions within a series of 60 consecutive billet extrusions. To this end, the transition zone was collected and segmented at 50 mm intervals along a 4000 mm distance from the stop mark.

To characterize the charge weld evolution, the segmented samples underwent a sequence of preparation steps, which involved grinding with silicon carbide abrasive papers of 500, 1000, and 2000 grit in a wet environment. This was followed by rough polishing using diamond spray abrasives with particle sizes of 9, 3, and 1 μm applied on a short-nap cloth. The final stage involved polishing the specimens using a silicon dioxide (SiO_2) suspension on a short-nap cloth. The specimens were immersed in an etching solution for 600 s, which consisted of a 30% sodium hydroxide solution, heated to 60 °C, followed by dipping in distilled water and acetone.

Following specimen preparation, the quantitative assessment of charge weld evolution was carried out by calculating the percentage area of the new billet as a function of distance from the stop mark, as depicted in Fig. 2. Subsequently, three samples were chosen from the charge weld zone, representing the early, mid, and late stages, in order to investigate both the evolution of microstructure and mechanical behaviors. The new material percentages for the selected samples were found to be 42%, 67.5%, and 96%, respectively.

The microscopic observations were performed using the Hirox rH 2000 Digital Microscope and the FEI Quanta 650 FEG Scanning Electron Microscope (SEM), with a particular emphasis on the charge weld zone. The SEM was used with an accelerating voltage of 10 kV for back-scattered electron (BSE) imaging. Additionally, compositional analysis was conducted by SEM using Energy-Dispersive X-ray Spectroscopy (EDS), with an accelerating voltage of 10 kV.

The development of mechanical properties within the charge weld zone was explored through the Vickers hardness test, which was conducted using the Mitutoyo HM-200 series Microhardness Tester, employing a load of 0.2 kgf and a 10-second dwelling time. The hardness experiments were iterated 3 times for confirmation. Moreover, the Instron Multiaxial 250 kN universal testing machine was employed to conduct drift-expanding tests. The test setup was prepared in accordance with the ISO 8493:2004 drift-expanding test standard, as depicted in Fig. 3 [13]. These tests were carried out under quasi-static conditions at room temperature. To reduce frictional effects, a molybdenum-based commercial Molykote-Multilub grease was applied to the interface between the tube and the conical mandrel. Subsequently, the conical mandrel was driven through the tube at a constant speed of 0.5 mm/s, and the testing software recorded both compression force and distance during the tests.

Table 2
Extrusion parameters used in the extrusion experiments.

Billet diameter	203	mm
Billet length	750	mm
Billet temperature	460	°C
Temperature taper	40	°C/m
Ram speed	11.5	mm/s
Extrusion ratio	33	/
Container temperature	420	°C
Die temperature	450	°C

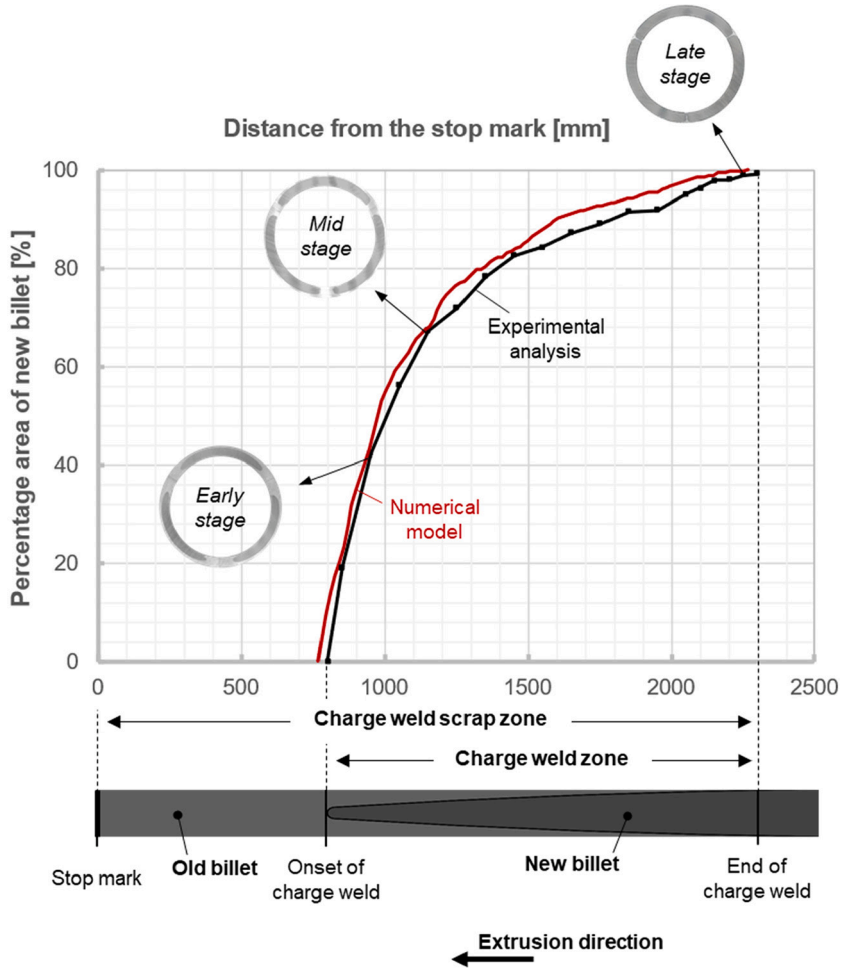

Fig. 2. Charge weld evolution derived from experimental characterization and numerical analysis.

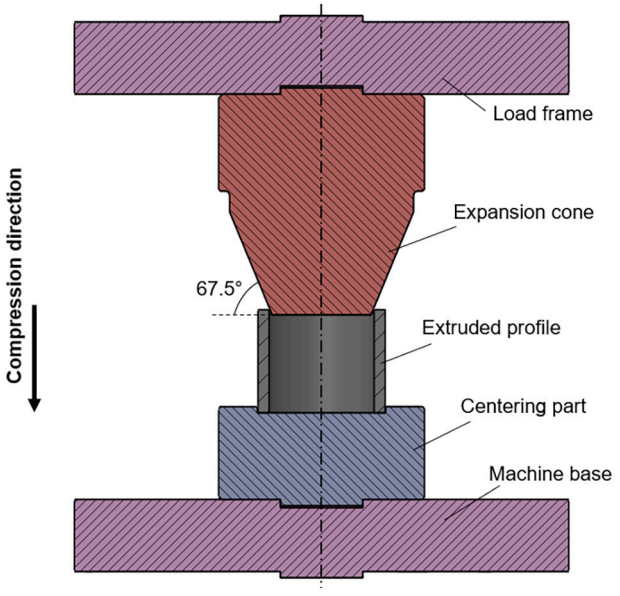

Fig. 3. Experimental setup of drift-expanding test.

2.3. Numerical modeling

To explore charge weld evolution, a numerical model was developed using a commercial FE software package, QForm-Extrusion 10.2.1. This software uses the Arbitrary Lagrangian-Eulerian (ALE) formulation combined with an implicit time integration scheme. As shown in Fig. 4,

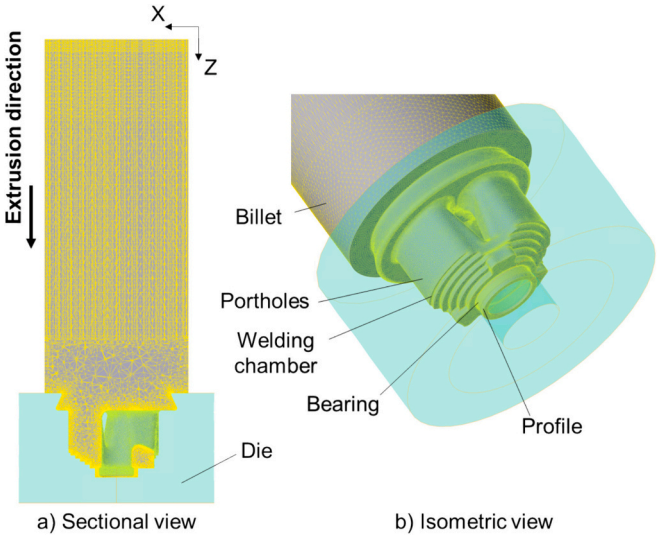

Fig. 4. Numerical model of aluminum extrusion.

the model components were categorized into four groups: the billet, portholes and welding chamber, bearing, and profile [14]. The extrusion tools were modeled as rigid bodies, with the billet being the sole deformable body within the model. Both the extrusion tools and billet were discretized using 3D tetrahedral 4-noded elements. In total, the model consisted of 288,102 surface elements, 3,250,756 volumetric elements and 600,618 nodes.

The flow stress of AA6060 material was described using the Sellars-Tegart inverse sine hyperbolic function [15], as given by:

$$\overline{\sigma} = \frac{1}{\alpha} sinh^{-1}\left[\left(\frac{Z}{A}\right)^{\frac{1}{n}}\right] = \frac{1}{\alpha} sinh^{-1}\left[\left(\frac{\dot{\varepsilon} exp(E_a/RT)}{A}\right)^{\frac{1}{n}}\right] \quad (1)$$

where $\overline{\sigma}$ is flow stress, and α, n and A are temperature-independent material constants, E_a is the activation energy, R is the universal gas constant, and T is the absolute temperature. The parameter values employed in the model were derived from a set of hot torsion tests conducted by Verlinden et al. [16]: E_a = 161 kJ/mol, R = 8.314 J/(K·mol), $\alpha = 0.035\ (\text{MPa})^{-1}$, $n = 4.67$, $A = 7.6301 \times 10^{10}\ \text{s}^{-1}$ and T is expressed in Kelvin.

The Levanov friction coefficient was used in the FE model with the formula proposed by Levanov [17], given by:

$$\tau_L = m\frac{\overline{\sigma}}{\sqrt{3}}\left[1 - exp\left(-L_n\frac{\sigma_n}{\overline{\sigma}}\right)\right] \quad (2)$$

In this equation, τ_L is the friction stress, m ($0 \le m \le 1$) is the friction constant, σ_n is the normal stress, $\overline{\sigma}$ is the equivalent flow stress and L_n is the Levanov coefficient. Following the findings of Bandini et al. [18], the Levanov coefficient was set to 1.25, and the heat transfer coefficient between the billet and the tool was set to 11,000 W/m^2 K. The remaining thermal and physical properties utilized in the model were set to the default values stored in the QForm database.

The formation of the charge weld was computed using a transient analysis approach implemented in QForm-Extrusion. The numerical model underwent an initial validation through a comparison with the findings from the conducted extrusion experiment, specifically focusing on extrusion force. Fig. 5 shows that the model provides high accuracy in capturing the maximum extrusion force, exhibiting a negligible difference of less than 1%. Similarly, the model closely resembles the minimum extrusion force, with a deviation of around 3%. Although negligible, this slight error could be attributed to the change in the deformation zone and stress state at the end of extrusion process, particularly in relation to the butt-end [19]. Secondly, the model accurately captures the trend in the evolution of the charge weld. Remarkably, the numerical model accurately predicts the end of the charge weld, with an error of less than 1.5% (Fig. 2). Further details on the validation of the numerical analysis of charge weld evolution can be found in the study by Sariyarlioglu et al. [5].

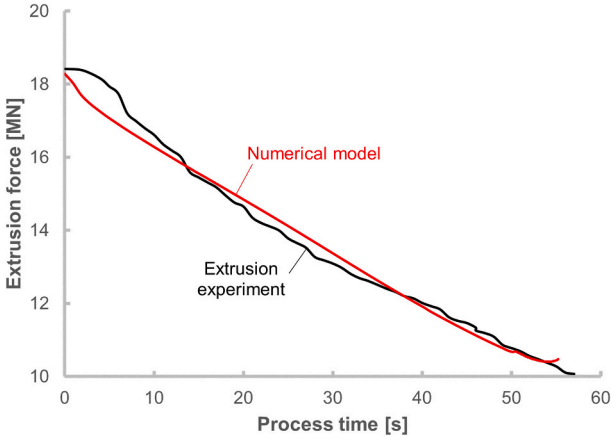

Fig. 5. Analysis of extrusion force difference between experimental and numerical analysis.

3. Results and discussion

3.1. Microstructural investigations

The microstructural evolution was explored throughout the progression of charge weld formation. Fig. 6 provides digital microscopy observations capturing both the mid and late stages of charge weld development. Specifically, Fig. 6a and Fig. 6b present the charge weld interface between the new and old materials, while Fig. 6c and Fig. 6d reveal the etched groove and holes at the interface during the mid and late stages, respectively. It can be observed that there is a noticeable decrease in both the distribution and size of the grooves and holes as the charge weld progresses. This observation is consistent with findings reported by Valberg [1], pointing out that the local pressure between mating surfaces of new and old materials leads to contact with each other. Subsequently, a solid-state pressure welding process initiates, resulting in charge weld formation. This welding process involves the crushing and fragmentation of oxide particles, accompanied by a reduction in the size of surface irregularities, thus contributing to the observed decrease in the sizes of grooves and holes. Consequently, the decrease in groove and hole dimensions here is claimed to be attributed to the increased local pressure between the two material surfaces during the progression of the charge weld in the extrusion process.

Furthermore, the charge weld interface of the mid-stage sample was examined using SEM in BSE imaging mode. As depicted in Fig. 7a, the charge weld zone exhibits a dense distribution of particles in dark vision. Subsequent to this visual observation, EDS analysis was executed on the region indicated in Fig. 7b to ascertain the chemical composition of the interested area in the charge weld zone. The results reveal a predominant presence of oxygen (O) elements, in alignment with the alloying elements of aluminum (Al), magnesium (Mg), and silicon (Si). Additionally, traces of chromium (Cr), manganese (Mn), zinc (Zn), copper (Cu), iron (Fe), and titanium (Ti) elements were detected in the zone. This indicates the presence of impurities within the charge weld zone. Consequently, it can be inferred that the impurities and oxide particles are distributed within the aluminum alloy matrix in the charge weld zone.

3.2. Hardness distribution along the charge weld

The hardness distribution across the charge weld zone in the samples obtained from mid-stage and late-stage conditions was examined. Standard deviations for each measurement, acquired through three repetitions, are slightly over ±1.5 HV. The average hardness values derived from these three repeated measurements in both new material and old material regions are presented in Fig. 8**.** Notably, the maximum difference between the average values was recorded at 10.2 HV, signifying a lack of significant hardness variations between new material and old material within the charge weld zone. This finding aligns with the observations by Den Bakker et al. [3]. Moreover, the analysis reveals a consistent hardness distribution throughout the progression of the charge weld.

3.3. Charge-weld strength along the charge weld zone

To analyze the evolution of charge-weld strength along the charge weld zone, a set of drift-expansion experiments was conducted using the setup indicated in Section 2.2. As shown in Fig. 9, the compression force-hoop strain graphs were captured for samples extracted from the early, mid and late stages of the charge weld progression. These experiments were carried out until the compression distance reached approximately 38 mm, which depended on the length of the specimens.

The hoop strain was calculated using the equation of $(D_f - D_i)/D_i$, where D_f is the final inner diameter of the tube and D_i is the initial inner

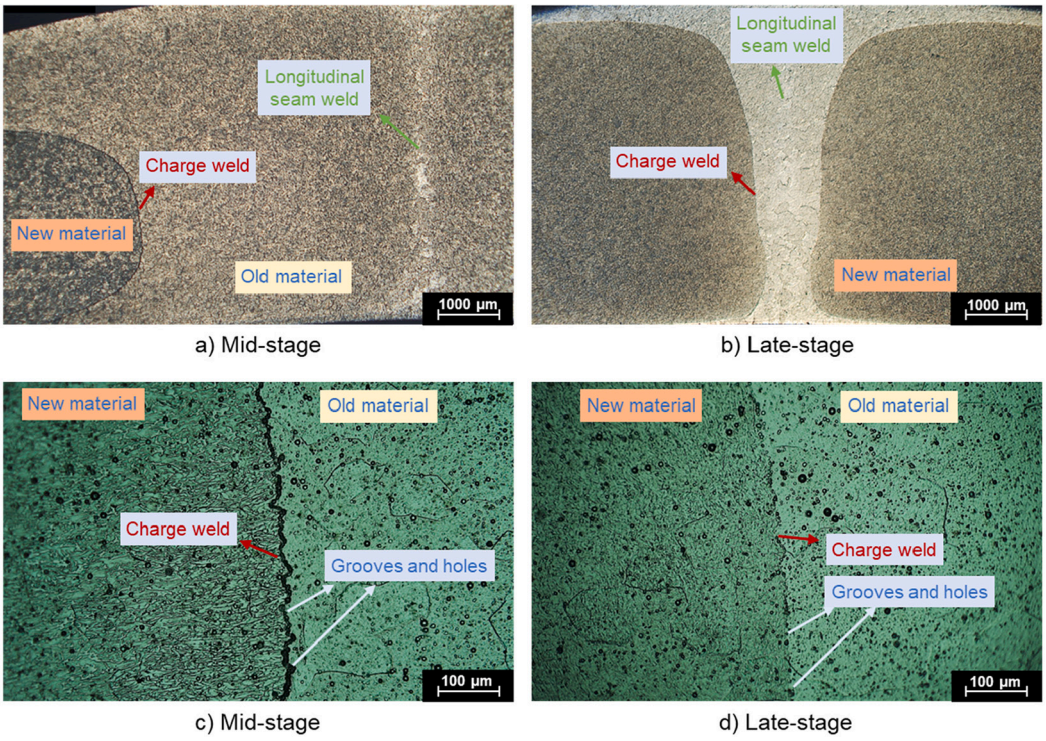

Fig. 6. Microstructural evolution of charge weld at different stages.

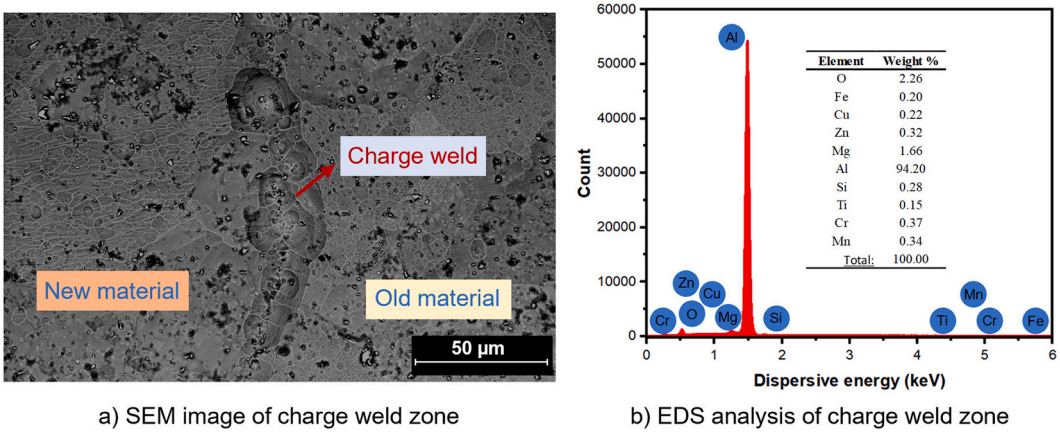

Fig. 7. Microstructural examination of the charge weld at the mid-stage.

diameter of the tube. The tubular samples were expanded until the hoop strain reached 0.6 mm/mm, while no complete fracture occurred in these samples. Instead, the initiation of fracture can be observed on the cross-sections of early-stage and mid-stage samples. Remarkably, as shown in Fig. 10, for the same applied hoop strain, it was observed that the size of the fracture initiation zone was more substantial at the early-stage sample in comparison to the mid-stage of the charge weld progression, while no fracture initiation was detected at the late-stage sample.

To delve into the evolution of charge-weld strength during the charge-weld progression, a numerical investigation was undertaken by back-tracing the thermo-mechanical histories of the six points positioned on the front face of the profile. Fig. 11 illustrates the positional alignment of tracking points and corresponding streamlines resulting from this backtracking process. During the aluminum extrusion process, the material flow occurs under conditions of elevated pressure and velocity. Building on the discussion in the previous section, the interplay between pressure and material flow stress is pivotal in forming extrusion welds. This process, which refers to solid-state welding, leads to crushing and fragmentation of oxide particles, as well as a reduction in surface irregularities, thereby enhancing welding strength.

Various methods have been documented in the literature for assessing longitudinal seam weld quality in extrusion. In this study, the approach proposed by Plata and Piwnik [20], referred to as the pressure-time (Q) criterion, was employed to analyze the evolution of charge-weld strength. This criterion is grounded in the integral over time of the mean stress, normalized by the actual effective stress, along a path for a welding element [21]. The criterion is expressed as follows,

$$Q = \int_t \frac{p}{\sigma}\, dt \tag{3}$$

where the p denotes the mean stress and σ represents the effective stress.

The charge weld formation within the extrusion die was calculated

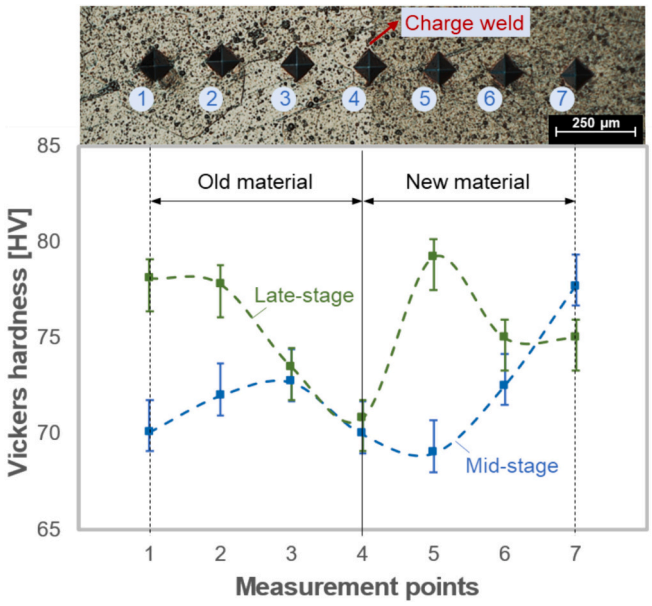

Fig. 8. Hardness distribution within charge weld zone.

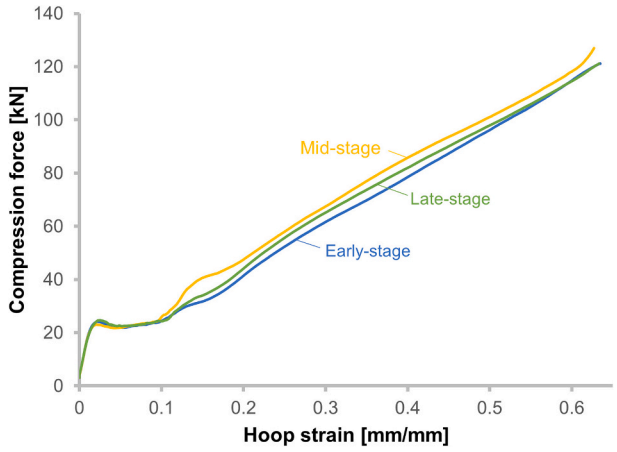

Fig. 9. Drift-expanding test findings.

up to the point where new material reached the bearing surface area using the velocity of each tracked point, as shown in Fig. 11. The gradual formation of the charge weld was illustrated based on this computation with a time interval of 0.3 s. This figure also shows the inhomogeneous nature of material flow within the extrusion die. It is noted that P1 presents slower material flow due to friction between the deforming material and the die, leading to the formation of the end of the charge weld. Conversely, P3 and P4 show faster material flows, resulting in the formation of the tip of a tongue-shaped charge weld.

Subsequently, the *Q*-values were calculated through each streamline (P1-P6) using Eq. (3), as shown in Fig. 12. Here, it was assumed that the butt-end was sheared off at the end of each ram stroke before mating two consecutive billets. The findings reveal that metal flows near the die walls (P1 and P6), present higher Q-values compared to those of P2-P5, indicating a potential positive influence on charge-weld quality. Consequently, when considering both the velocity of each tracking point and their respective Q-values, the charge-weld quality may improve as the charge weld progresses. This is consistent with the results of the drift-expanding tests.

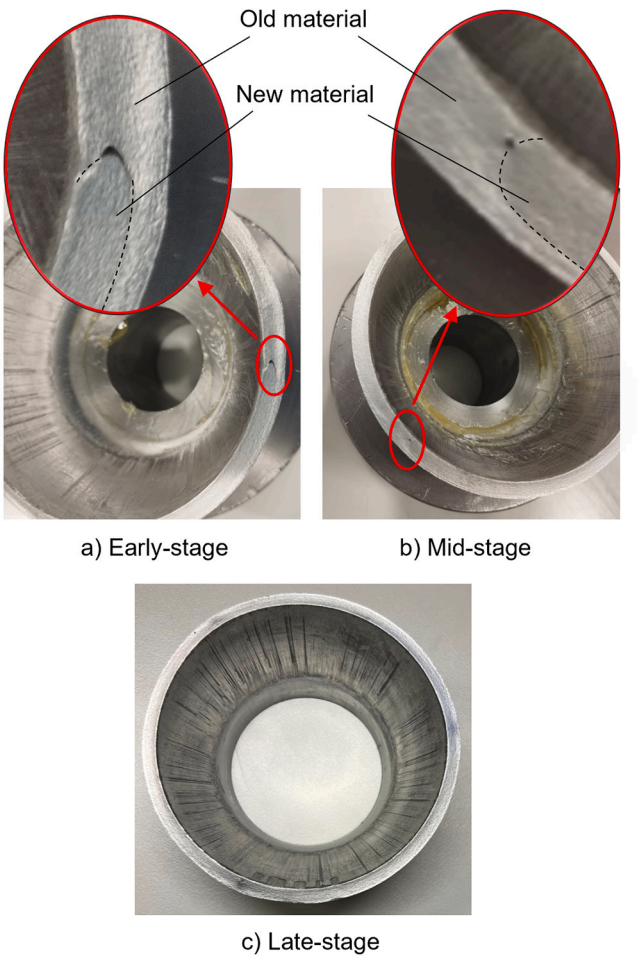

Fig. 10. Fracture initiation on the sample surfaces.

4. Conclusions and outlook

This paper presents new insights into the mechanisms driving the evolution of material integrity within the charge weld zone in hot extrusion of aluminum hollow profiles, through industrial-scale extrusion experiments, microstructural and mechanical characterization, and numerical investigation. The observations suggest that the presence of oxide particles, as well as other impurity elements that have the potential to compromise material integrity, was noted in the charge weld zone. Moreover, a reduction in both the distribution and size of grooves and holes was identified as the charge weld progressed in extrusion; however, the hardness distribution between new and old materials within the charge weld zone does not show a remarkable difference. Drift-expanding experiments reveal that the fracture initiation size is more substantial in the early-stage compared to the mid-stage of charge weld progression under a hoop strain of 0.6 mm/mm, without obvious fracture initiation detected in the late-stage. A backtracking analysis and pressure-time weld strength assessment based on numerical simulation suggest that charge-weld quality improves as the charge weld progresses, aligning with drift-expanding experimental results.

In conclusion, the findings of this study provide a deeper understanding of material integrity evolution within the charge weld zone and highlight the importance of developing a reliable criterion of material integrity in aluminum hollow extrusion. Further work will focus on more quantitative characterization and modeling of microstructural and mechanical evolution to enhance the understanding and control of material integrity issues induced by charge weld for more sustainable extrusion of value-added aluminum profiles.

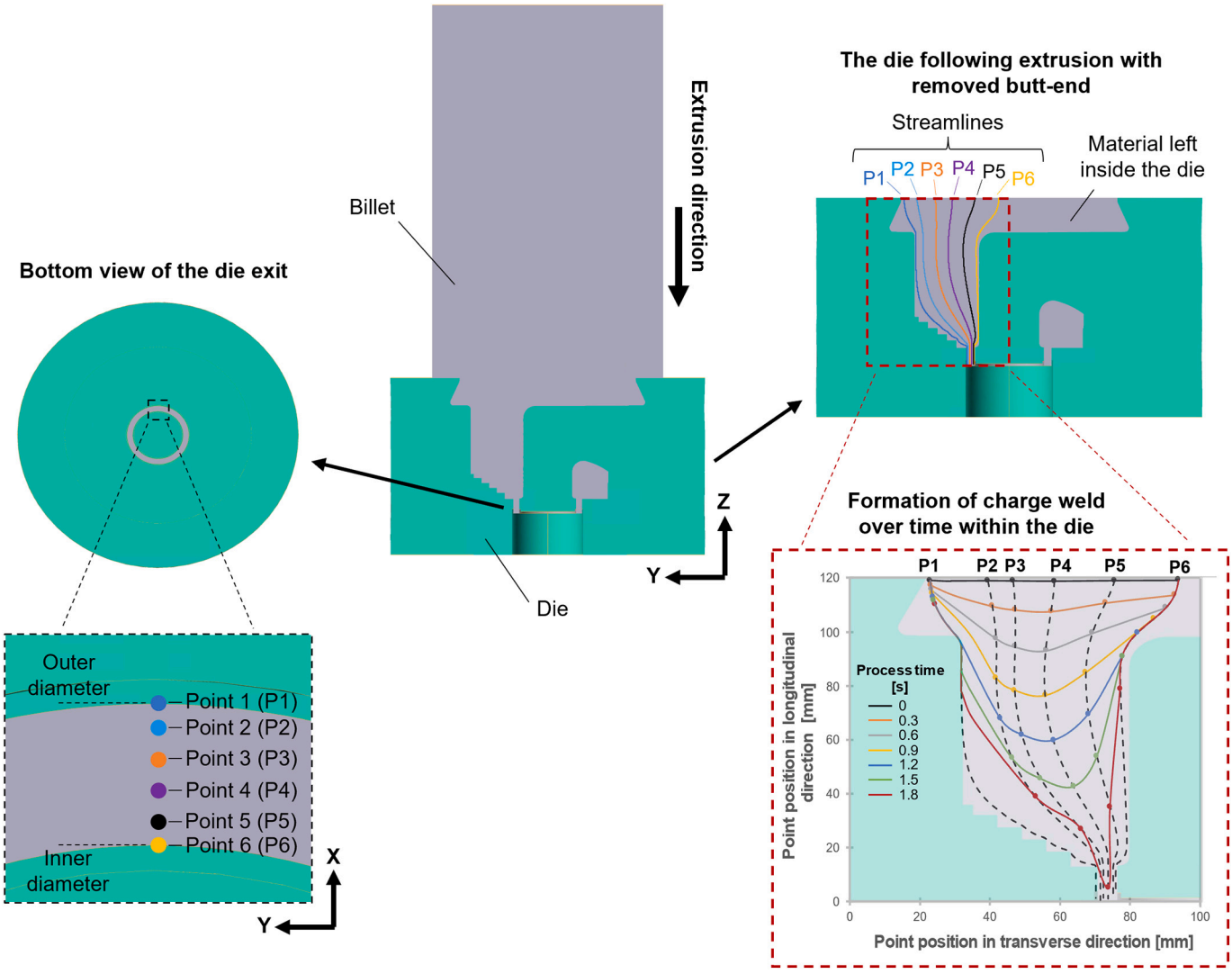

Fig. 11. Left side shows the position of tracking points. Top right side displays the streamlines traced backward in time. Bottom right side illustrates how a charge weld forms inside the extrusion die over time.

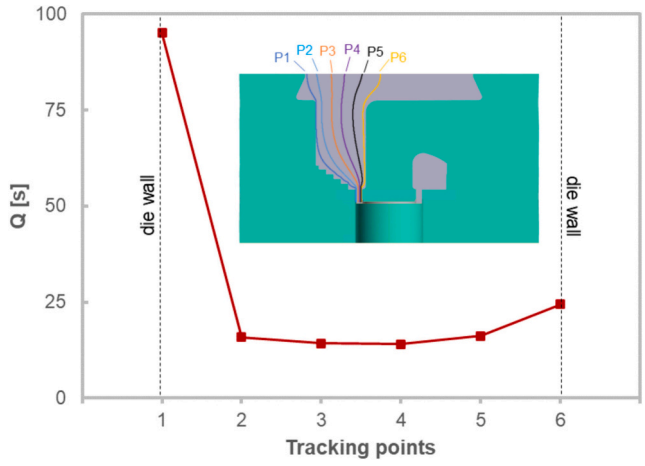

Fig. 12. Calculated Q-values through each streamline.

Consent for publication

This work is original and has not been published elsewhere nor it is currently under consideration for publication elsewhere.

CRediT authorship contribution statement

Eren Can Sariyarlioglu: Formal analysis, Investigation, Methodology, Validation, Visualization, Writing – original draft. **Torgeir Welo:** Conceptualization, Methodology, Project administration, Resources, Supervision, Writing – review & editing. **Jun Ma:** Conceptualization, Investigation, Methodology, Supervision, Writing – review & editing.

Declaration of competing interest

The authors declare no competing interests.

Acknowledgements

The authors gratefully acknowledge the financial support from the Norwegian University of Science and Technology (NTNU), NTNU Aluminum Product Innovation Center (NAPIC), and the EXPECT project [No.: 321571] and AluGreen project [No.: 328831] sponsored by

Research Council of Norway. In addition, the authors would like to thank Benteler Automotive Raufoss AS (Raufoss, Norway) for their support with extrusion experiments.

References

[1] Valberg H. Extrusion welding in aluminium extrusion. Int J Mater Prod Technol 2002;17(7):497. https://doi.org/10.1504/IJMPT.2002.001317.
[2] Sheppard T. Extrusion of aluminium alloys. 1999. https://doi.org/10.1007/978-1-4757-3001-2.
[3] Den Bakker AJ, Katgerman L, Van Der Zwaag S. Analysis of the structure and resulting mechanical properties of aluminium extrusions containing a charge weld interface. J Mater Process Technol Mar. 2016;229:9–21. https://doi.org/10.1016/j.jmatprotec.2015.09.013.
[4] Oberhausen G, Zhu Y, Cooper DR. Reducing the environmental impacts of aluminum extrusion. Resour Conserv Recycl Apr. 2022;179:106120. https://doi.org/10.1016/j.resconrec.2021.106120.
[5] Sariyarlioglu EC, Negozio M, Welo T, Ma J. Charge weld evolution in hollow aluminum extrusion: experiments and modeling. CIRP J Manuf Sci Technol Apr. 2024;49:14–27. https://doi.org/10.1016/j.cirpj.2023.12.007.
[6] Loukus A, Subhash G, Imaninejad M. Mechanical properties and microstructural characterization of extrusion welds in AA6082-T4. J Mater Sci 2004;39:6561–9.
[7] Zhang X, Feng D, Shi X, Liu S. Oxide distribution and microstructure in welding zones from porthole die extrusion. Trans Nonferrous Met Soc Chin Mar. 2013;23(3):765–72. https://doi.org/10.1016/S1003-6326(13)62527-3.
[8] Ren X, Zhang JL, Li JP, Liu J, Zhang HH, Wang XR. Microstructural characterization of extrusion welds in 6xxx aluminum alloys. 2015.
[9] Zhang C, Dong Y, Wang C, Zhao G, Chen L, Sun W. Evolution of transverse weld during porthole extrusion of AA7N01 hollow profile. J Mater Process Technol Oct. 2017;248:103–14. https://doi.org/10.1016/j.jmatprotec.2017.05.017.
[10] Yu J, Zhao G, Zhao X, Chen L, Chen M. Microstructures of longitudinal/transverse welds and back-end defects and their influences on the corrosion resistance and mechanical properties of aluminum alloy extrusion profiles. J Mater Process Technol May 2019;267:1–16. https://doi.org/10.1016/j.jmatprotec.2018.12.006.
[11] Oberhausen G, Cooper DR. Modeling the strength of aluminum extrusion transverse welds using the film theory of solid-state welding. SSRN Electron J 2023. https://doi.org/10.2139/ssrn.4488657.
[12] Spittel M, Spittel T. Part 2: Non-ferrous alloys - light metals · WE 43. 2011. p. 178–82. https://doi.org/10.1007/978-3-642-13864-5_26.
[13] International Organization for Standardization. Metallic materials - Tube - Drift-expanding test. EN ISO 8493:2004; 2004.
[14] Sariyarlioglu EC, Negozio M, Ma J, Welo T, Ringen G. Effect of die design on charge welds in aluminium extrusion. 2024. p. 468–78. https://doi.org/10.1007/978-3-031-41023-9_48.
[15] Sellars CM, McG.-Tegart WJ. Hot workability. Int Metall Rev Jan. 1972;17(1):1–24. https://doi.org/10.1179/imtlr.1972.17.1.1.
[16] Verlinden B, Suhadi A, Delaey L. A generalized constitutive equation for an AA6060 aluminium alloy. Scr Metall Mater Jun. 1993;28(11):1441–6. https://doi.org/10.1016/0956-716X(93)90496-F.
[17] Levanov AN. Improvement of metal forming processes by means of useful effects of plastic friction. J Mater Process Technol Dec. 1997;72(2):314–6. https://doi.org/10.1016/S0924-0136(97)00191-X.
[18] Bandini C, Reggiani B, Donati L, Tomesani L. Code validation and development of user routines for microstructural prediction with Qform. Mater Today Proc 2015;2(10):4904–14. https://doi.org/10.1016/j.matpr.2015.10.052.
[19] Kraft FF, Gunasekera JS. Conventional hot extrusion. In: Metalworking: Bulk forming. ASM International; 2005. p. 421–39. https://doi.org/10.31399/asm.hb.v14a.a0004006.
[20] Plata M, Piwnik J. Theoretical and experimental analysis of seam weld formation in hot extrusion of aluminum alloys. In: Proceedings of seventh international aluminum extrusion technology seminar ET; 2000. p. 205–11.
[21] Donati L, Tomesani L. The prediction of seam welds quality in aluminum extrusion. J Mater Process Technol Nov. 2004;153–154(1–3):366–73. https://doi.org/10.1016/j.jmatprotec.2004.04.215.